Proceedings of the 12th International Conference on
Aluminium Alloys, September 5-9, 2010, Yokohama, Japan

pp. 2156-2161

Consolidation of rapidly solidified aluminum alloy powder by high pressure torsion

Hiroki Adachi[1], Akiei Tanaka[2], Jun Kusui[2] and Zenji Horita[3]
[1]Department of Materials Science and Engineering, Kyoto University, Yoshida Hommachi, Sakyo-Ku, Kyoto, 606-8501, Japan.
[2]Toyo Aluminum K. K., Hino, Shiga, 341-14, Japan
[3]Department of Materials Science, Kyushu University, 744 Motooka, Nishi-Ku, Fukuoka, 819-0395, Japan

Consolidation of rapidly solidified aluminum alloy powder was carried out using a High Pressure Torsion (HPT) process at room temperature. The fabricated powders were Al-9.5Zn-3Mg-1.5Cu-0.04 Ag (Meso10) and Meso10-1.3Zr (MZ13) in mass%. Each powder was strained by 10 rotations of an anvil, and consolidated into disks with a diameter of 10 mm. A dislocation cell structure was observed in the center of a Meso10 disk, and an ultra-fine grained structure with a diameter of 100-200 nm was observed in the fringe of the disk. On the other hand, in both the center and edge of a MZ13 disk, an ultra-fine grained structure was observed. No precipitates were detected by XRD in any of the as-processed disks. After aging at 383 K, a coarse stable η phase precipitated in all disks, although a metastable η' phase generally precipitated in the Al-Zn-Mg series alloys during aging at 383 K. During aging of the Meso10 disk, the hardness decreased monotonically because recovery occurred with precipitation, reducing the dislocation density. On the other hand, in the MZ13 disk, age hardening was observed.

Keywords:*Aluminum alloy, Rapidly solidified powder, Consolidation, High pressure torsion, Zr.*

1. Introduction

Powder metallurgy (P/M) allows the fabrication of rapidly solidified powders, which can contain solutes exceeding the equilibrium solubility limit [1]. Meso10 and MZ13 aluminum alloys were developed using P/M methods [2-4]. The tensile strength of T6-treated Meso10 and MZ13 are reported to be 790 and 879 MPa, respectively. The typical chemical compositions are Al-9.5Zn-3Mg-1.5Cu-0.04Ag and Al-9.5Zn-3Mg-1.5Cu-0.04Ag-1.33Zr in mass%. These alloy powders, fabricated by an air-atomization method, were consolidated by hot extrusion at 773 K. The reason for using hot extrusion was to strengthen the bonding between particles in the powder by destroying the alumina layer formed on the particle surfaces. However, when using hot extrusion to consolidate the powder, the rapidly solidified structure was broken by the heat load due to phase decomposition. Therefore, in this research, consolidation of rapidly solidified powders at room temperature was carried out using high-pressure torsion (HPT) processing, which is a severe plastic deformation (SPD) process. In the HPT process, which has a high grain refining ability, torsion deformation is applied along with high-pressure compression [5-7]. The microstructural change induced by the HPT process was investigated, and its correspondence with mechanical properties was studied.

2. Experimental

Meso10 and MZ13 alloy powders were fabricated by air-atomization at Toyo Aluminum K.K.. The cooling rate was estimated to be $2\sim5\cdot10^5$ K/s [2]. The powders were collected after sieving to below 150 μm. HPT was conducted with an applied pressure of 8 GPa. Each powder was strained by 10 rotations of an anvil, at a rotation speed of 1 rpm, and then consolidated into disks with a diameter of 10 mm and a thickness of 0.2 mm. The disks were aged at 383 K. The powders, HPT processed

disks, and aged disks were mechanically polished to a mirror-like surface, and the micro Vickers hardness was measured along center-to-fringe radii. A load of 0.49 N was applied for 15 s using an Akashi MVK-E micro Vickers hardness tester.

The microstructural changes with HPT processing and T6 aging were evaluated by scanning electron microscopy (SEM), transmission electron microscopy (TEM), and X-ray diffraction (XRD). SEM observations were conducted for the powders and HPT-processed samples using a JEOL JSM-6500F field emission scanning electron microscope at an accelerating voltage of 10 kV. TEM observations were conducted for HPT-processed and aged samples. Disks 3 mm in diameter were punched out and mechanically polished to a thickness of 0.1 mm. The specimens were electro-polished by a twin-jet polisher with a solution of 66% HNO_3 and 34% CH_3OH at 243 K. The specimens were observed using a Phillips CM200F field emission transmission electron microscope at an accelerating voltage of 200 kV. XRD measurements were conducted for the powders, HPT-processed samples, and aged samples using a Brucker AXS D8 DISCOVER X-ray diffractometer with Cu Kα radiation.

3. Experimental results and discussion

3.1 Atomized powder

Figure 1 shows backscattered electron images of Meso10 and MZ13 atomized powders. A typical dendritic structure was shown in all powders, and no precipitate was observed in any of the powders. In the dendritic arms, because the backscattered electron intensity was comparatively high, the Zn, Cu, and Zr atoms with atomic numbers higher than that of Al were considered to be segregated. It has been reported that there are one or a few grains in the atomized Al-Zn-Mg series alloy powders [8]. Figure 2 shows XRD profiles of Meso10 and MZ13 atomized powders. In both powders, only two diffraction peaks were observed, from $(111)_{Al}$ and $(200)_{Al}$, and it was confirmed that the particles had not crystallized during the atomization process and that the atomized powders had a solid solution state.

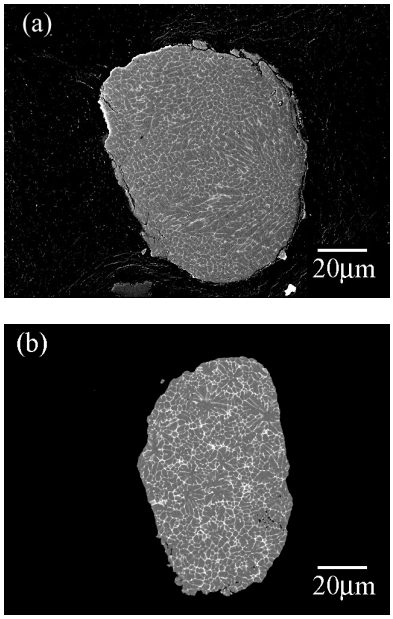

Fig.1 SEM micrographs of (a)Meso10 and (b)MZ13 atomized powders.

Figure 3 shows the full width at half maximum (FWHM) of $(111)_{Al}$ diffraction peaks. The FWHM from the MZ13 powder was higher than that of the Meso10 powder. This was because the lattice constant increased in the dendrite arms when the added Zr atoms segregated, increasing the difference between the lattice constants of the arm and inter-arm regions.

3.2 HPT processed samples

Figure 4 shows backscattered electron images of HPT-processed Meso10 and MZ13 samples. Although some voids with diameters of about 1 μm were observed in the samples, it was confirmed that the powders had combined with each other, and that this consolidation was possible in the HPT process. Dendtric structures were still observed in the center of the HPT-processed Meso10 sample, and in the powder. On the other hand, no dendritic structure was evident in the fringe. This was because

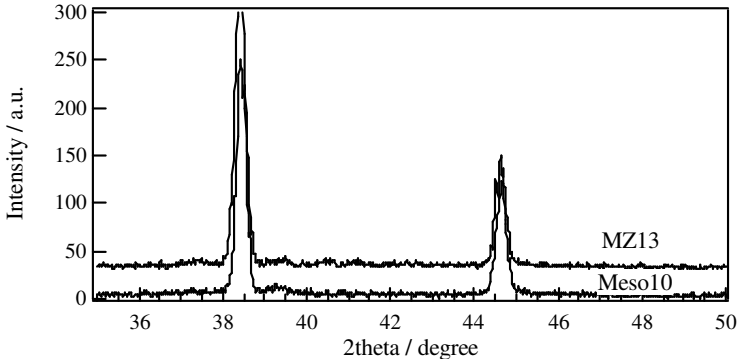

Fig.2 XRD patterns of Meso10 and MZ13 atomized powders.

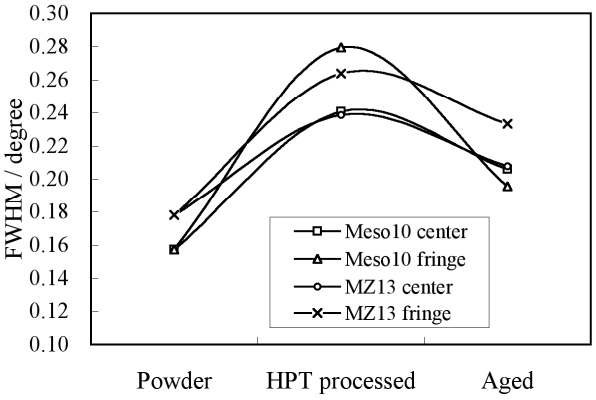

Fig.3 FWHM of $(111)_{Al}$ diffraction peaks from powders, HPT-processed samples, and samples aged at 383K for 360ks.

the shear strain introduced by the HPT process increases in proportion to the radius, and the dendritic arms were fragmented by the large shear strain in the fringe. On the other hand, in both the center and fringe of the MZ13 sample, fragmented dendtric arms were observed. Figure 5 shows TEM images and selected area electron diffraction (SAED) patterns from HPT-processed Meso10 and MZ13 samples. In the center of the Meso10 sample, coarse grains containing a number of tangled dislocations were observed. In the fringe, since Debye rings were observed, ultra-fine grains were present and had randomly distributed crystal orientations. The refinement of grain size was achieved, reaching a grain size of 100-200 nm, because the shear deformation was remarkably large in the fringe of the sample.

On the other hand, in MZ13 samples after HPT, since Debye rings were observed in both the fringe and the center, ultra-fine grains with random orientations were distributed over the entire samples. Since the grain refinement by HPT occurred by grain subdivision of initially coarse grains, the fragmentation of dendritic arms also occurred in regions containing ultra-fine grains after HPT. In all samples after HPT, no precipitated phase was observed, and no peaks except for $(111)_{Al}$ and $(200)_{Al}$ were detected by XRD, as shown in Fig. 6. There was no formation of a new phase during the HPT process, and the samples after HPT remained in a supersaturated solid solution state. As indicated in Fig. 3, the FWHM of the $(111)_{Al}$ peak increased during the HPT, and the amount of increase in the fringe was larger than that in the center. This was because the increase in FWHM derived from an increase in lattice defect density and a decrease in crystallite size. Although the grain size in the center of the MZ13 sample was finer than that of MZ13 after HPT, the FWHM increase in Meso10 by HPT was larger than that of MZ13. This implies that the dislocation density had a stronger effect on FWHM change during HPT than grain size did, in this case. Therefore, although the grain size in the center of the Meso10 sample after HPT was coarser than that of MZ13, the dislocation density was significantly higher

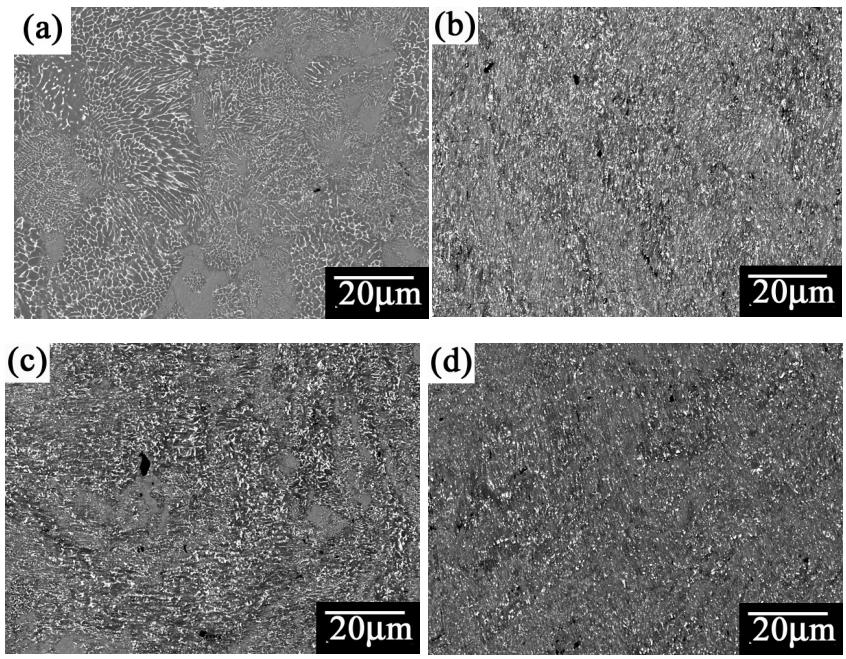

Fig.4 SEM micrographs of HPT-processed samples at the (a) center, (b) fringe of Meso10, and at the (c) center and (d) fringe of MZ13.

Figure 7 indicate the Vickers hardness of the powders and HPT processed samples. At the powder state, the hardness of Meso10 is larger than that of MZ13. This is caused by the increase of solid solution hardening by the addition of 1.3 mass% Zr. By HPT process, the hardness remarkably increases and the amount of increase is 137.3HV in the center of Meso10 and 131.9HV in the center of MZ13 and 181.6HV in

the fringe of Meso10, 157HV in the fringe of MZ13, respectively. The hardness increase in the fringe is larger than that in the center and it is considered that the grain refinement and the increase of dislocation density by the increase of shear strain from the center to fringe contribute the hardness increase. The hardness increase of Meso 10 is larger than that of MZ13 both in the center and fringe. This is because the increase of dislocation density of Meso10 by HPT process is larger than that of MZ13 as is clear from the change of FWHM. As the result of the hardness increase by HPT process, Meso10 samples have 218.7HV in the center and 263.5HV in the fringe, respectively. Meso10 is classified into 7000 series aluminum alloy and it is reported that η' metastable phase precipitate and the precipitation hardening occur during T6 aging treatment. The maximum hardness of aged Meso10 extrudate is reported to be 210HV[9]. Though there is no precipitate in HPT processed Meso10 sample as is clear from TEM and X-RD measurement, the HPT processed Meso10 sample have the hardness which is higher than the conventional Meso10 extrudates.

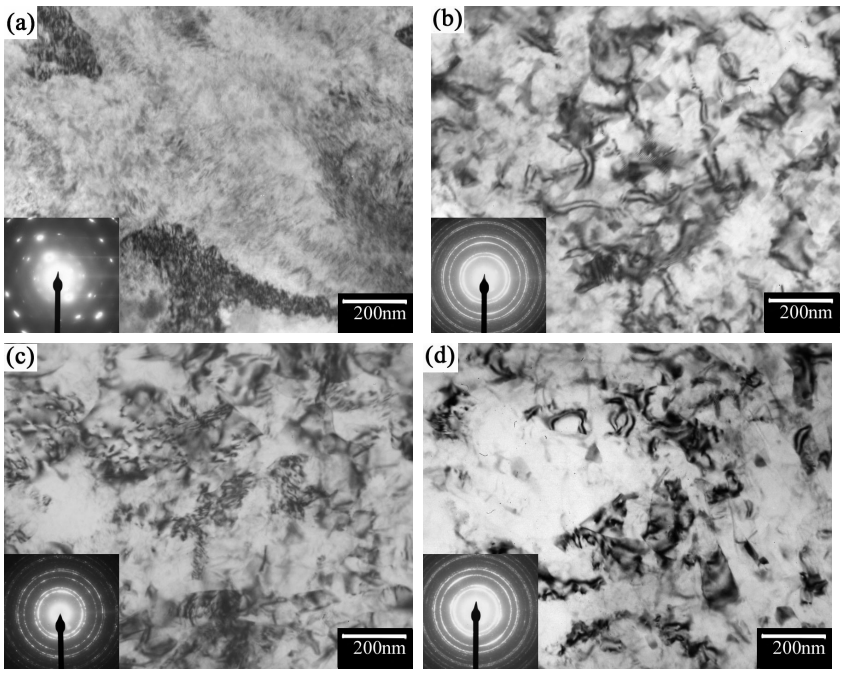

Fig.5 TEM micrographs and diffraction patterns of HPT-processed samples at the (a)center, (b)fringe of Meso10, and at the (c)center and (d)fringe of MZ13.

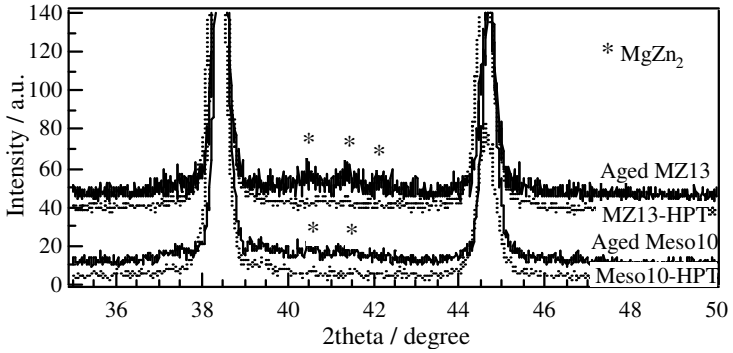

Fig.6 XRD patterns of HPT-processed Meso10, aged Meso10, HPT-processed MZ13, and aged MZ13 samples, from the bottom to the top. The aged samples were aged at 383K for 360ks.

3.3 Aged samples

Figure 8 shows the Vickers hardness change with 383 K aging. In the center of the Meso10 sample, the hardness remained relatively unchanged for 10.8 ks, and then increased gradually. On the other hand, in the fringe of the Meso10 sample, the hardness monotonically decreased with aging. In both the center and the fringe of the MZ13 sample, the hardness gradually increased with aging, and a maximum aging hardness of 270.3 HV was attained after 36 ks of aging. The hardness increase by aging was 9.8 HV in the center of Meso10, and 16.3 HV and 12.7 HV

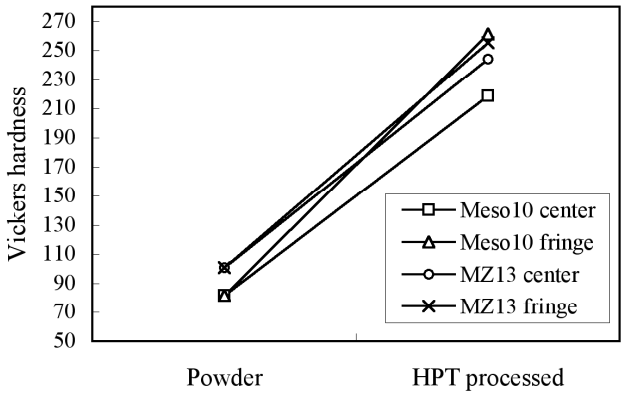

Fig.7 Vickers hardness of powders and HPT-processed samples.

in center and fringe of MZ13, respectively. The hardness increase of MZ13 was larger than that of Meso10, and the hardness increase in the center tended to be larger than at the fringe.

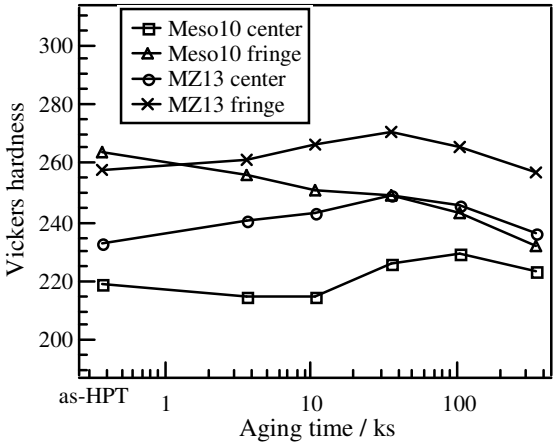

Fig.8 Vickers hardness change of Meso10 and MZ13 samples by 383K aging.

Figure 9 shows TEM micrographs of samples aged at 383 K for 360 ks. In all samples, no remarkable coarsening was observed and the grain size remained ultra-fine in the fringe of Meso10, the center of MZ13, and the fringe of MZ13. In the center of the Meso10 sample, many precipitates about 20 nm in diameter were distributed in the matrix. Although it is not clearly observed due to the strong contrast of the ultra-fine grains, precipitates of equivalent size were also detected in the fringe of Meso10, the center of MZ13 and the fringe of MZ13, as indicated in the black arrows in Figure 9(d). It has been reported that the η' metastable phase, with a diameter of about 5 nm, precipitates by aging under the same conditions (383K, 360ks) in Meso10 extrudate. The metastable η' phase is semi-coherent to the matrix, and the age-hardening by the η' phase was 80 HV in Meso10 extrudate. Compared to the diameter of this η' phase, the diameter of the precipitate formed in the HPT-processed samples was quite large, and the age-hardening of HPT-processed samples was much less than that of Meso10 extrudate.

The diffraction peaks of the $MgZn_2$ phase can be detected at a diffraction angle of $2\theta = 40\sim42$ degrees in the X-ray diffraction profiles of aged Meso10 and MZ13 samples, as shown in Fig. 2. This indicates that the coarse precipitates with a diameter of about 20 nm shown in the aged samples were $MgZn_2$. $MgZn_2$ is the η stable phase, and is incoherent to the matrix. Generally, during 383 K aging, η stable phase does not precipitate because of the high activation energy for the precipitation, but η' metastable phase, which has low activation energy, does precipitate. However, since a very high density of dislocations was introduced in the HPT-processed samples, and because these dislocations acted as preferential nucleation sites, the activation energy for the precipitation of η phase decreased, and the η phase precipitated more easily. Since it has been reported that the contribution to age-hardening by an incoherent phase is smaller than that of a coherent phase, and the amount of age-hardening is inversely proportional to the diameter of precipitates, the extent of age-hardening by coarse incoherent η phase was much less than in Meso10 extrudate.

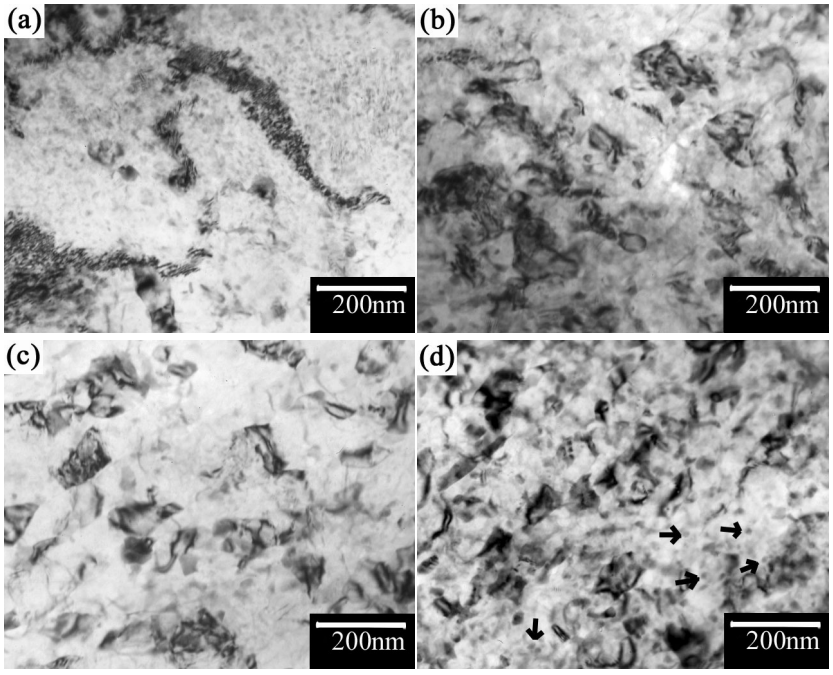

Fig.9 TEM micrographs of sample aged at 383K for 360ks in the(a)center of Meso10, (b)fringe of Meso10, (c)center of MZ13, and (d)fringe of MZ13.

Figure 3 shows the FWHM change with aging. The FWHM decreased after aging at 383 K for 360 ks. Since no remarkable coarsening of the grains was observed, these decreases were considered to result

from the decrease in dislocation density. In the fringe of the Meso10 sample, because of the large FWHM decrease, the decrease in dislocation density was considered to be large, and the corresponding hardness decrease was also large. As a result, in the fringe of Meso10, the weakening of the work-hardening was exceeded by the increase in precipitation hardening by the η phase, and age-softening was observed. On the other hand, in the center of the Meso10 sample, since the hardness decrease by the decrease of dislocation density is comparable to the hardness increase by the precipitation hardening of the η phase, the hardness remained relatively unchanged till 36 ks of aging. In the MZ13 sample, compared to the Meso10 sample, the decrease in FWHM tended to be small. This indicates that the decrease in dislocation density due to aging was small. Since supersaturated Zr atoms reduce the dislocation mobility, the annihilation of dislocations became rare, and the rate of dislocation density decrease by aging slowed. As a result, in the MZ13 sample, the decrease of work-hardening was comparatively small, and age-hardening was observed from the beginning of aging.

4. Summary

1. Rapidly solidified aluminum alloy powders of Meso10 and MZ13 were consolidated into disk-like samples using an HPT process.
2. The HPT-processed samples remained in the solid solution state and had no precipitation. In the center of the Meso10 sample, coarse grains with high-density dislocations were observed. On the other hand, in MZ13 and at the fringe of Meso10, an ultra-fine grained structure with a diameter of 100-200 nm was observed. The hardness increased to 263.5 HV because of work hardening and a grain refining effect in the fringe of Meso10.
3. During aging at 383 K, a coarse η stable phase precipitated in the matrix. In the center of the Meso10 sample, since the decrease of work hardening by recovery exceeded the increase by precipitation hardening, the hardness monotonically decreased with aging. On the other hand, in MZ13, since Zr solutes prevented recovery, the decrease by work hardening was comparatively small, and age hardening was observed. As a result, the hardness increased to 270.3 HV in the fringe of MZ13.

5. References

[1] S. Hori, S. Saji and A.Takehara: *Proc. 4th Int. Conf. on Rapidly Quenched Metals*, Ed. by T. Masumoto and K. Suzuki, (Sendai, 1981) pp. 1545-1548.
[2] H. Adachi, K. Osamura, S. Ochiai, J. Kusui and K. Yokoe: Scripta mater. 44(2001) 1489-1492.
[3] H. Adachi, K. Osamura, K. Kikuchi and J. Kusui: Mater. Trans. 46(2005) 211-214.
[4] H. Adachi, K. Osamura, J. Kusui and S.Okaniwa: Mater. Sci. Forum 519-521(2006) 1479-1484.
[5] Z. Horita and T. G. Langdon: Mater. Sci. Eng. A 410-411(2005) 422-425.
[6] G. Sakai, Z. Horita and T. G. Lanfdon: Mater. Sci. Eng. A 393 (2005) 341-351.
[7] Y. Ito and Z. Horita: Mater. Sci. Eng. A 503(2009) 32-36.
[8] Y. Morimoto, H.Adachi, K.Osamura, J. Kusui and S. Okaniwa: Mater. Sci. Forum 519-521(2006) 1623-1628.
[9] K. Osamura, H. Adachi, J. Kusui and K.Yokoe: *LiMAT-2001*, Ed. by N. J. Kim, C.S. Lee and D. Eylon, (Pusan, 2001) pp. 597-602.